

Chapter 7. Oceanic Internal Waves and Solitons

John R. Apel¹

Global Ocean Associates, Silver Spring, Maryland, USA

7.1 Introduction

Internal waves are, as their name implies, waves that travel within the interior of a fluid. Such waves are most familiar as oscillations visible in a two-layer fluid contained in a clear plastic box often sold in novelty stores. In the box, two immiscible and differently colored fluids fill the entire volume; when the box is tilted or otherwise disturbed, a slow large amplitude wave propagates along the interface between the fluids. This internal wave has its maximum amplitude at the interface, and has vertical displacements of zero at the top and bottom. The wave owes its existence to the stratified density structure of the two fluids, with a very sharp density change occurring along the interface and with the properties that the smaller the density contrast, the lower the wave frequency, and the slower the propagation speed [Apel, 1987].

Similar modes exist within the geophysical fluids of the atmosphere and ocean. Solar radiation is absorbed in the near surface ocean layers, resulting in warmer water and lower density in that region, thereby resulting in a stratified fluid. Upper ocean temperature and salinity gradients are relatively sharp under most conditions and any excitation or disturbance of the pycnocline (a zone where density changes maximally) will tend to propagate away from the region of generation as an internal wave [Apel, 1987].

The particular type of internal wave most often observed is termed a *solitary wave* or *soliton*. Solitary waves are a class of nonsinusoidal, nonlinear, more-or-less isolated waves of complex shape that occur frequently in nature. These waves maintain their coherence, and hence visibility, through nonlinear hydrodynamics and appear as long, quasilinear stripes in imagery. The internal wave signatures are made visible by wave/current interactions; wherein the near-surface current associated with the internal wave locally modulates the surface wave height spectrum. Primary modulations typically occur at wavelengths ranging from a few meters to between 10 cm and 50 cm, but secondary interactions further transport surface wave energy down to sub-centimeter scales. Thus, a roughening of the short-wave portion of the surface wave spectrum takes place in regions of internal wave phase where the currents are convergent. At a distance of one-half of an internal wave's phase to the rear of a depression wave, the sea surface has been swept relatively clean of surface wave energy and the ocean in this phase region is very flat.

The earliest recognition of internal waves appears to have been made by *J. Scott Russell* [1838, 1844] who reported on the formation of a single, unchanging hump or mound in the shallow water of the Scottish Canal, generated when a towed barge was brought to a sharp halt in the canal. Russell followed the wave for several miles on horseback until he lost it in the windings of the canal. Later *Korteweg and deVries* [1895] derived some of the interesting mathematical properties of such a wave and produced their now-famous soliton solutions.

¹This chapter was produced from material authored by Dr. John R. Apel. The primary source of material was Nonlinear Solitary Internal Waves by J. R. Apel and D. M. Farmer, Global Ocean Associates (GOA) Report 2000-2 September 2000, with additional material taken from [Apel, 1987, Apel, 2000 and Apel and Worcester, 2000]. The editors contributed some additional material, primarily to Section 2.2 Remote Sensing of Coherent Internal Solitons.

Subsequent attention to solitary waves had been given mainly because of their strange and interesting mathematical characteristics. Recently, however, it has been the recognition of the widespread occurrence of internal waves in the ocean that has spurred geophysically-oriented investigations; including studies not only of the internal hydrodynamics, but also of their impacts on surface wave spectra, air-sea interaction, remote sensing science, shallow-water acoustics, and coastal mixed-layer dynamics.

Reports of what are almost certainly surface manifestations of oceanic internal solitary waves are centuries, if not millennia old, but the scientific study of the phenomenon is more recent. For example, it has been known for over 150 years that in the island archipelagos of the Far East, long, isolated stripes of highly agitated features that are defined by audibly breaking waves and white water are occasionally seen on the surface of the sea [Wallace, 1869]. These features propagate past vessels at speeds that can exceed two knots. The features are often seen in deep water and are not usually associated with any nearby bottom feature to which their origin might be attributed. In the nautical literature and charts, they are sometimes identified as “tide rips.” In Arctic and sub-Arctic regions, especially near the mouths of fjords or rivers flowing into the sea, analogous waves of lower energy may have been observed as long ago as Roman times with reports of “sticky water,” but have certainly been a recognized phenomenon—dead water—since Viking times [Ekman, 1904].

Internal solitary waves are important for many practical reasons. They are ubiquitous wherever strong tides and stratification occur near irregular topography. As such, they are often prominent features in optical and radar satellite imagery of coastal waters. They can propagate over several hundred kilometers and transport both mass and momentum. Indeed, an early motivation for studying internal waves was the unexpectedly large stresses they impose on offshore oil-drilling rigs. Internal waves are often associated with a net change in stratification in which case they are referred to as travelling internal undular bores. Their propagation carries with them considerable velocity shear that can lead to turbulence and mixing. The mixing often introduces bottom nutrients into the water column, thereby fertilizing the local region and modifying the biology therein.

This chapter examines the signatures of internal waves in synthetic aperture radar (SAR) imagery. To help understand these signatures, the discussion includes material on the inherent characteristics, mechanisms of generation, and global distribution of internal waves. Our survey is necessarily brief and therefore frequent reference is made to the literature.

7.2 Observations

In-situ observations of internal solitons can be made using almost any ocean instrumentation capable of recording current, density, displacement of planktonic layers, or similar measurements. However, it has been remote sensing, both satellite radar and optical, that has brought about the realization of the widespread existence of internal solitons and provided the major impetus for their study.

7.2.1 Characteristics of Oceanic Solitary Internal Waves.

Internal solitons occur in stratified coastal waters as groups or packets of oscillations, with the number of cycles varying from a very few to a few dozen, depending on age and distance from generation point. They are usually produced by tidal currents flowing normal to the local bathymetry. Such processes are statistically quite reproducible given the same season,

the same phase of both the daily and fortnightly tides, and the bathymetry.

One often observed type of wave packet is usually characterized by several dominant features. The individual oscillations are nonsinusoidal, with predominantly downward displacements (i.e., depression internal waves); the amplitudes are rank-ordered, with the largest at the front of the packet and the smallest at its rear; the wavelengths and the crest lengths are also rank-ordered, with the longest waves again at the front of the group. The number of individual oscillations within the packet increases as its age increases, with one new oscillation added per Brunt-Väisälä period. The Brunt-Väisälä, or buoyancy period, describes the oscillation of a water parcel about its equilibrium depth, is used as a parameter to express the strength of stratification in a fluid. These wave packets are consistent with the Korteweg-de Vries equation, which approximately describes the dynamics. Additionally, the maximum amplitude of the leading oscillations appears to be related to the magnitude of the downward displacement of the pycnocline during the ebb (offshore) tidal phase.

A schematic of internal wave features is shown in Figure 7.1. Here are sketched two individual packets, the rightmost one having just been generated by offshore tidal flow at the shelf break within the last few hours, and the leftmost one being about 12 hours older and having been generated on the previous semidiurnal tide, and then propagating up onto the continental shelf on the order of 25 to 35 km from its formative point. This implies a phase speed of about 0.6 to 0.7 m s⁻¹, although phase speed needs to be carefully defined in terms of the theoretical models

Figure 7.1 shows both a vertical section of displacement and a horizontal plan of the wave crests. The vertical section shows that the displacements are mostly negative, and that the downward oscillations of the pycnocline are followed by a several-hour average depression of the density interface to the rear of the oscillatory region. A slow recovery of the pycnocline then takes place near the trailing edge of the undulation.

Typical scales for summertime continental shelf internal waves are given in Table 7.1. It should be emphasized that these characteristics are canonical, and any individual realization of a soliton packet can be expected to deviate from the ideal by significant factors.

Figure 7.2 shows an ERS-1 synthetic aperture radar image of four continental shelf soliton packets northeast of the Hudson Canyon off New York, generated during the previous 50 hours of tidal action at the shelf break. Such data, together with in-situ observations, have gone into making up the canonical description of the wave field.

The proper view of these soliton groups is that they are oscillations of the leading edge of an undulatory internal bore, or nonlinear internal tide on the shelf. Both observational evidence and numerical models of nonlinear hydrodynamics under these conditions show that the linear deep-sea barotropic tides (where the stratification structure of the water column remains intact) are transformed into nonlinear baroclinic tides (where the stratification structure of the water column is altered) as they move onto the shelf. Later, after several tidal cycles, dissipative forces reduce the nonlinearities to small values, so that near the shoreline, the tides are once again sinusoidal.

Soliton packets are also generated by tidal flow over relatively shallow sills or banks. While the generation process is probably similar to that at the continental shelf break, the subsequent evolution of the individual packets can be considerably different. Instead of encountering ever-decreasing water depths, the sill-formed soliton radiates into a deeper sea, and is less controlled by bathymetry (although depths continue to play a role as long as they are

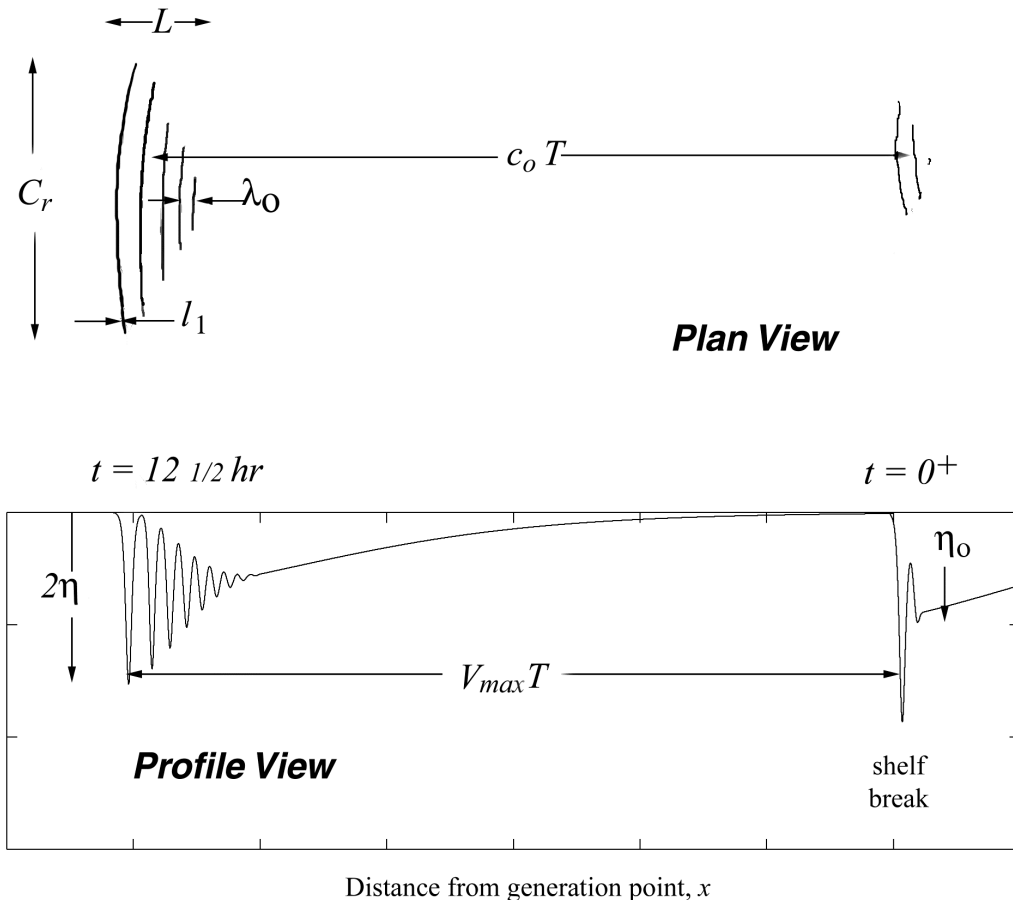


Figure 7.1. Schematic showing tidally-generated solitons on the continental shelf. $V_{\max}T$ is the internal tidal wavelength; c_0T is distance between packet centroids.

Table 7.1. Typical scales for continental shelf solitons

Characteristic	Symbol	Scale
Packet Length	L (km)	1 – 10
Amplitude Factor	$2h_0$ (m)	-15
Upper Layer Depth	h_1 (m)	20 – 35
Lower Layer Depth	h_2 (m)	30 - 200
Long Wave Speed	c_0 (m s ⁻¹)	0.5 - 1.0
Maximum Wavelength	λ_{MAX} (m)	100 – 1000
Crest Length	C_r (km)	0 - 30
Internal Tidal Wavelength	$D = VT$ (km)	15 – 40
Characteristic Soliton Width	l_1 (m)	100

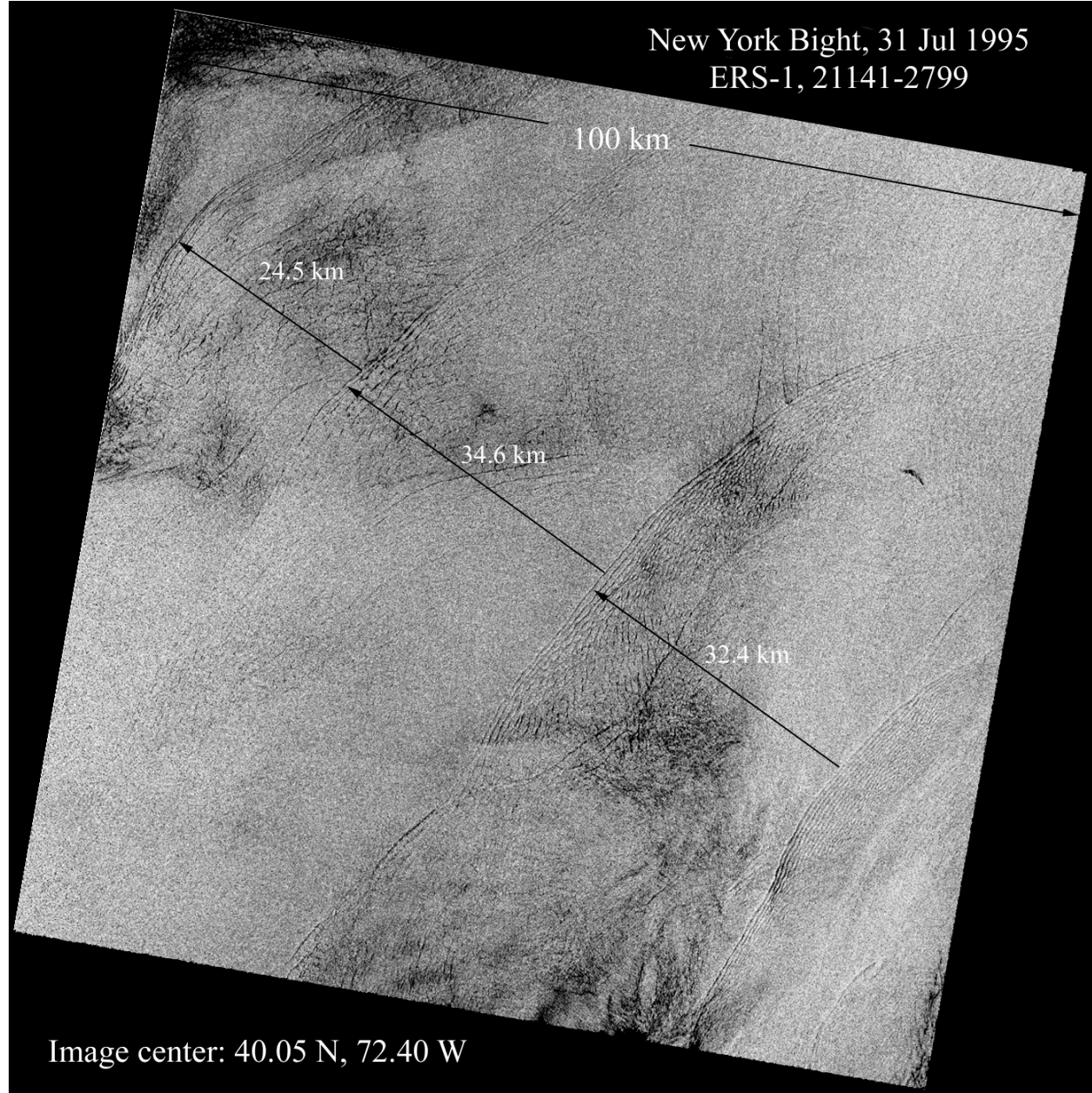


Figure 7.2. ERS-1 (C-Band, VV) SAR image of the New York Bight acquired on 31 July 1995. Four packets of tidally-generated internal waves are visible north of the Hudson Canyon, which lies near the bottom center of the image. Distance between packets is set by 12-½ hr semidiurnal tidal period. The imaged area is approximately 100 km x 100 km. Original Image ©ESA 1995

roughly less than the soliton wavelength). The restrictions in the Strait of Gibraltar, i.e. the Camarinal and Spartel Sills, are generation regions of great importance for the western Mediterranean and regularly produce solitons with amplitudes of 50 m to 100 m and wavelengths of 2 km to 4 km [Farmer and Armi, 1988; Armi and Farmer, 1988; Brandt et al., 1996].

Figure 7.3 shows a packet of solitons radiating eastward from the Strait of Gibraltar, having been formed by intense westward tidal flow across the Camarinal Sill several hours earlier. Such packets reach at least 200 km into the western Mediterranean Sea and exist for more than two days before decaying toward background levels [Apel, 2000]. Similar situations

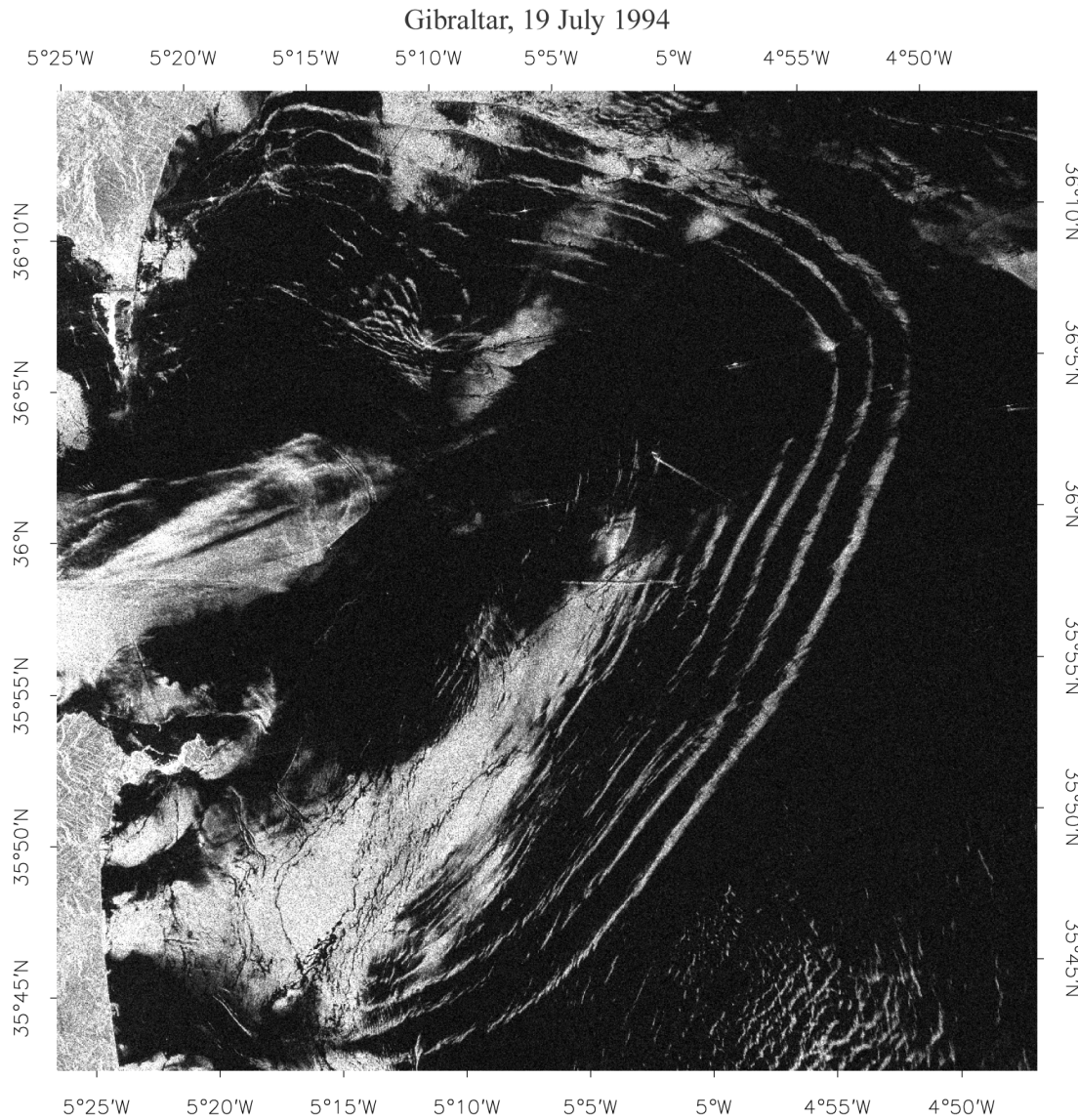


Figure 7.3. ERS-1 (C-band, VV) SAR image just east of Strait of Gibraltar, showing a large packet of solitons propagating into the Alboran Sea. The lead soliton is approximately 80 km from the generation region near the Camarinal Sill. Imaged area is 50 km × 50 km. Original image ©ESA 1994.

occur in the Sulu Sea in the Philippines [Apel and Holbrook, 1983; Apel *et al.*, 1985; Liu *et al.*, 1985], the strait between Luzon and Taiwan [Hsu and Liu, 2000a; Hsu and Liu, 2000b], and the arcs of the Andaman and Nicobar Islands in the eastern Indian Ocean [Apel, 1979; Osborne and Burch, 1980; Alpers *et al.*, 1997]. In the western tropical Pacific, the pycnocline depths are in excess of 100 m and, therefore, these sill regions are sources of intense internal solitons whose amplitudes can exceed 100 m and whose wavelengths can grow as large as 20 km.

7.2.2 Remote Sensing of Coherent Internal Solitons

Figures 7.2 and 7.3 show a few examples of internal waves detected using ERS SAR satellites. Because internal waves are coherent processes, they can be recognized in photographs

of the sea surface, in multispectral radiometer images, in real and synthetic aperture radar images, and in side-by-side plotting of repeated echo-soundings made in the water. Even the unaided eye at sea level can detect the induced surface-wave changes as rough and smooth regions. Remote sensors, however, with their Olympian view, provide a much broader picture of the horizontal distribution of the solitons than can be obtained by any other means. When enhanced by in-water measurements, it is possible to derive a nearly three-dimensional picture of internal waves, especially if aided by theoretical models of both the internal hydrodynamics and the surface wave-electromagnetic scattering processes. Internal waves were among the first oceanic phenomena to be studied with SAR. Even before the flight of space-based SARs, such waves had been identified in aircraft SAR imagery and analyses made of the variations in scattering cross section across the wave crests [Elachi and Apel, 1976].

In general, most internal waves exhibit the following characteristics that are observable in SAR imagery:

- They propagate in separate groups or "packets," with each packet being generated by the semidiurnal tidal cycle. The separation between packets can range from about 10 km up to 90 km.
- Each packet contains a few to a few dozen individual waves. Individual wavelengths can range from 100 m up to 20 km. Along the crest, lengths vary from 10 km to more than 100 km.
- The largest waves (in amplitude, wavelength, and along crest length) are found at the leading edge of the packet. The waves decrease in all aspects to the trailing edge.
- Wave signatures observed in SAR imagery are a series of alternating light/dark linear or curvilinear bands that represent the crests and troughs of the waves.

The light/dark signatures are the result of variations in sea surface roughness [Alpers, 1985]. Since a rough region of the ocean surface is an enhanced scatterer (See Chapter 2), the region appears bright in an image. Smooth regions appear darker, since the radar energy is more nearly specularly reflected away from the detector. The result is a characteristic signature of a lineal feature in SAR images typified by a bright region, then a dark region, and finally followed by normal roughness. Modulations of the surface wave spectrum can be quite strong. Under very low-wind conditions, it is not unusual for the smooth areas to provide essentially no signal to the detector.

For internal waves, the characteristic light/dark band signature (i.e., the alternating rough and smooth sea surface with the rough side leading) is caused by the generally down-going nature of the oscillations when the thermocline depth is smaller than the lower layer thickness. However, in shallow water, where the lower layer thickness becomes less than the upper layer, the polarization of the solitons becomes positive (i.e., internal waves of elevation) and the dark part of the phase leads the bright part, at least in principle. A similar phenomenon has been observed in the East China Sea [Liu *et al.*, 1998].

Figure 7.2 and Figure 7.4 show typical internal solitary wave packets in the New York Bight (the continental shelf off New York). The area is a prodigious source of internal solitons. The waves are generated by tidal flow near the edge of the continental shelf and occur in groups separated by about 20 km to 35 km, depending on the speed of propagation, which is typically between 0.5 m s^{-1} and 1 m s^{-1} on the shelf. Several field programs[‡] in this area have measured

[‡]SAR Internal wave Signature Experiment (SARSEX)-1984, [Gasparovic *et al.*, 1988]; Joint U.S./Russian Internal wave Remote Sensing Experiment (JUSREX)-1992, [Gasparovic and Etkin 1994]; Shallow Water Acoustics in Random Media (SWARM)-1995, [Apel *et al.*, 1997]

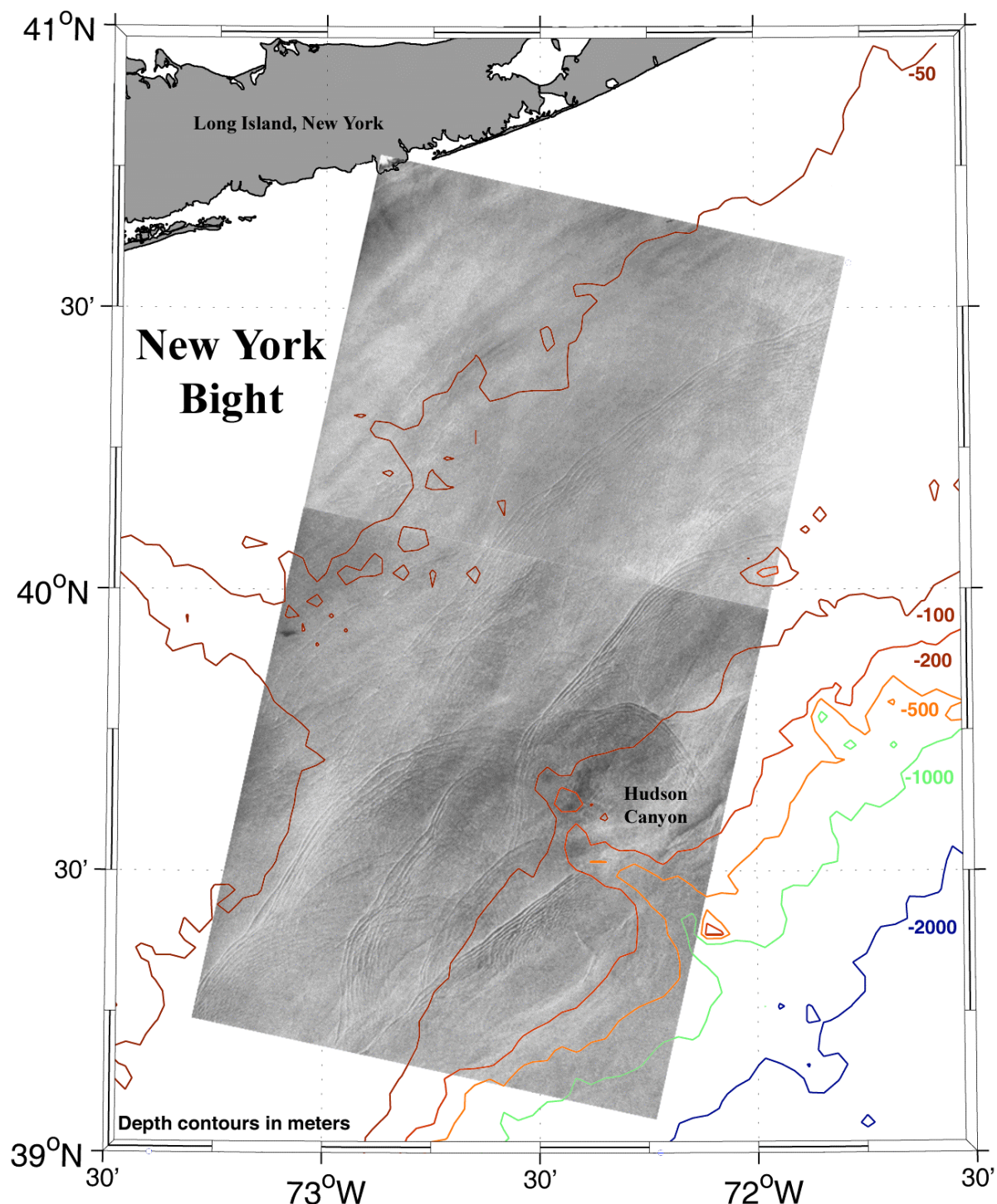


Figure 7.4. ERS-1 (C-band, VV) SAR images of the New York Bight acquired 18 July 1992 overlaid on a bathymetric chart [Smith and Sandwell, 1997]. The internal wave packets can be seen aligned roughly parallel with the local bathymetry. Original ERS-1 imagery ©ESA 1992.

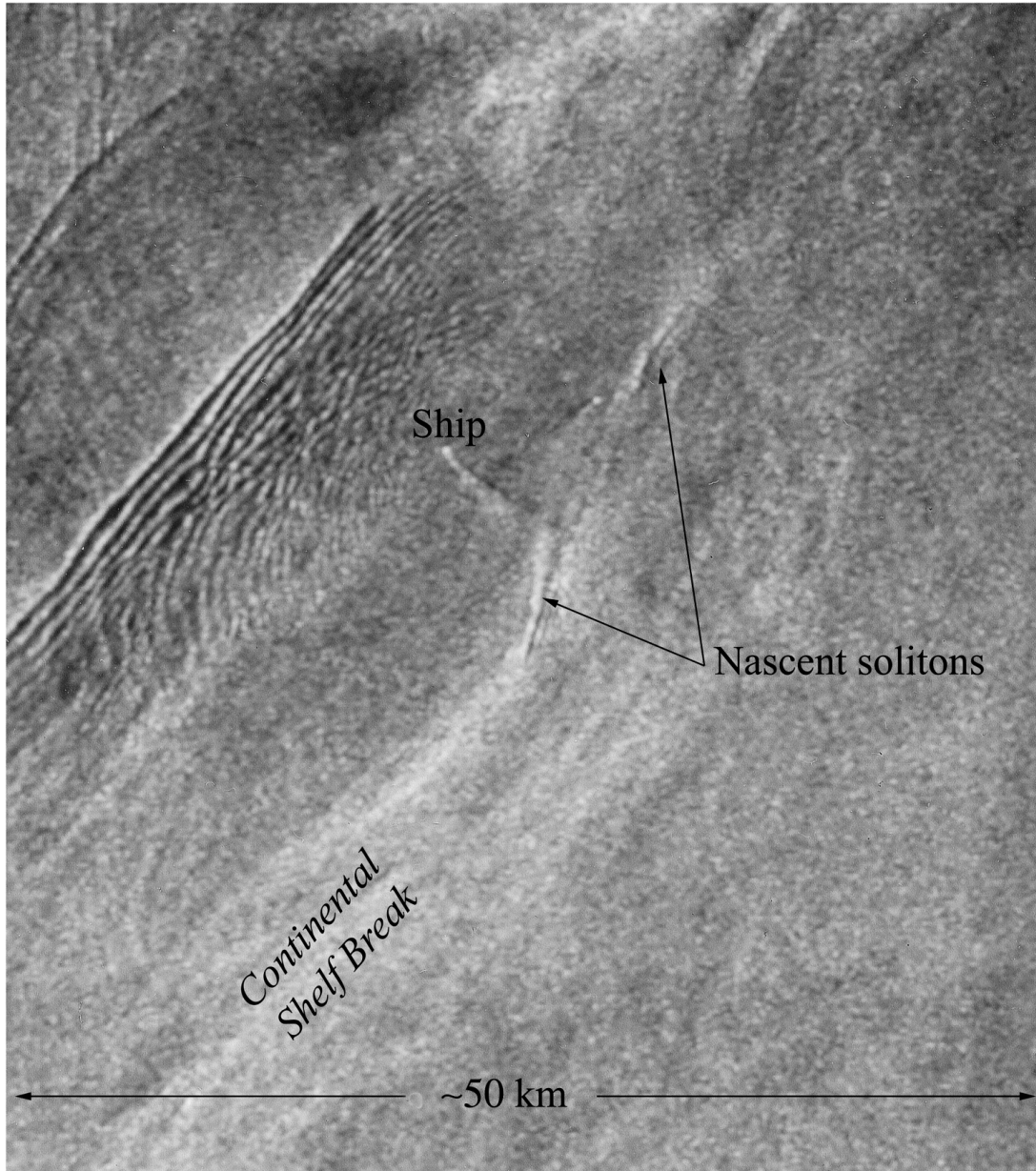


Figure 7.5. Solitons generated southwest of Hudson Canyon in the New York Bight, 18 July 1992. Nascent solitons are forming very near to the 200 m shelf break (cf. Figure 7.4) and will propagate toward the northwest. Original image ©ESA 1992.

soliton amplitudes between 5 m and 25 m, nonlinear phase speeds on the order of 0.65 m s^{-1} , and wavelengths from 200 m to over 1000 m. Figure 7.4 shows that north of the Hudson Canyon, the crests are strongly oriented along isobaths and have crest lengths in excess of 120 km. The groups shown in Figure 7.2 represent waves excited during the last four semidiurnal tidal cycles. It is thought that the waves form via some kind of lee-wave mechanism when the tidal flow is directed offshore, during which the flow leaving the edge of the continental shelf depresses the pycnocline by significant amounts. When the tide slacks, the depression moves onto the shelf and develops increasing numbers of oscillations—the solitons. Figure 7.5 is an enlargement of the segment of Figure 7.4 south of the Hudson Canyon. A nascent packet with one or two

oscillations is noted on the image; its position is very close to the shelf break, slightly inshore of the 200-m isobath. This demonstrates that the generation process takes place quite close to the shelf break.

Packets disappear as they approach shallow (typically 25 m to 40 m depth) water—approximately the upper layer depth, because of strong bottom attenuation. Just a few broken crests can be seen inside the 50 m isobath on Figure 7.4. Additionally, the phase velocities are reduced by both the shoaling and (usually) by the decreasing pycnocline depth as distance to shore decreases.

The result is that the distance between packets is reduced; in Figure 7.2, the spacing between the last two packets in the image is only about 25 km, as contrasted with the other packets, which are spaced about 35 km. South of the canyon, seven packets are visible, with interpacket separations near 15 km, suggesting possible generation on both ebb and flood semidiurnal tides.

At sills or other underwater barriers, the generation process is somewhat similar to that at the continental shelf break, but the details differ. During the ebb phase of the tide, either a lee-wave or a hydraulic jump tends to form on the down-current side of the sill. When the tide slacks and reverses, this depression is released, moves across the sill, and radiates into the space beyond, developing oscillations along its leading edge. These oscillations are the solitary waves.

Figures 7.6a through 7.6d present ERS-1 imagery of four different internal wave packets from the Strait of Gibraltar. They show the internal waves at different times in their life cycle (i.e., distances from the generation point). Figure 7.6a (24 March 1996) shows a newly formed soliton packet propagating through the Strait of Gibraltar. There are four fairly uniform oscillations that have wavelengths about 1½ km. Atlantic winds and long surface waves (light gray) are penetrating into the Alboran Sea about as far as the leading crest. In Figure 7.6b (12 June 1994) a soliton packet has broken free of the strait and radiates as a curved wavefront. The curvature is determined by a combination of refraction and tidal advection. The signature of the group is quite intense, in spite of what appears to be a strong surface wind over much of the western Mediterranean. To the east at a distance of roughly 25 km, another weak packet is slightly visible. Figure 7.6c (19 July 1994) shows a large packet advancing into the Alboran Sea with upwards of 10 or more solitons in the packet. The internal wave packets develop a new oscillation each buoyancy period and diminish in amplitude as time goes on. The center of the wavefront shows evidence of advection by large-scale current, probably tidal. Figure 7.6d (26 May 1994) shows a well-evolved soliton packet some 50 hours after generation. It has reached over 200 km from its formation region and developed over 30 oscillations. Spreading of the packet is caused by the range of amplitude-dependent phase speeds present [Apel, 2000; Apel and Worcester, 2000]. The ultimate eastern extent of the solitons in the Mediterranean has not been determined, although the present data show that soliton lifetimes are at least a few days, quite similar to the Sulu Sea [Apel *et al.*, 1985].

Figure 7.7 is another example of sill generated solitons from the Sulu Sea. Figure 7.7 is a composite of seven ERS-1/2 images collected during three overpasses (April 1996, July 1996 and January 1998). The Sulu Sea contains some of the oceans largest internal waves with observed amplitudes up to 90 m, speeds in excess of 2.0 m/s and lifetimes exceeding 2½ days [Apel *et al.*, 1985]. Like the Strait of Gibraltar, after generation the Sulu Sea waves propagate out into deeper water.

Figure 7.7 shows how the Sulu Sea internal wave packets evolve in terms of their wavelength, crest length, and number of solitons per packet. The lead soliton wavelength is

Oceanic Internal Waves and Solitons

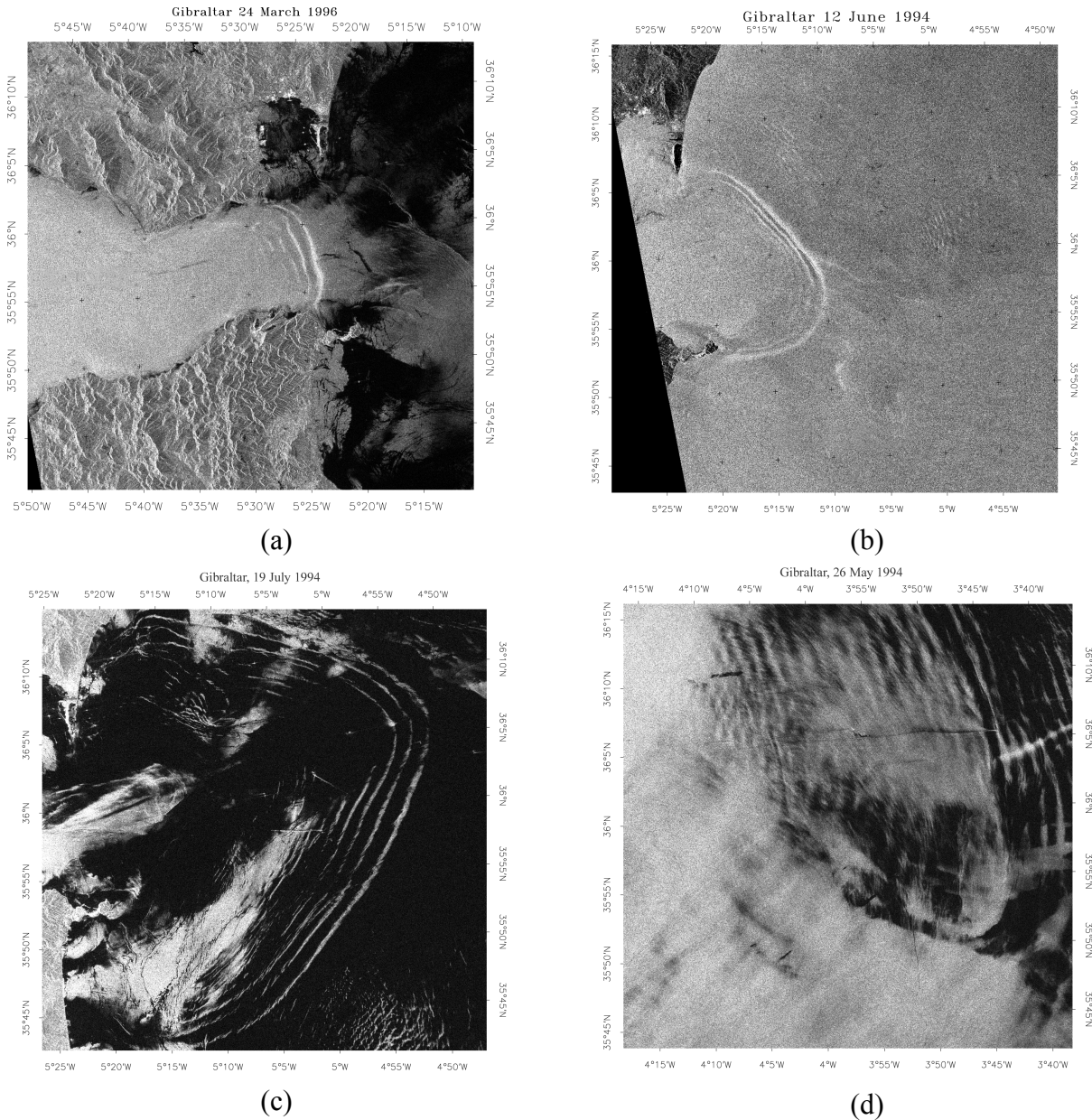


Figure 7.6. ERS-1 (C-Band, VV) SAR images showing internal wave packets in the Mediterranean at various distances from the generation point at the Camarinal Sill. Lead soliton distances are approximately a) 30 km, b) 55 km, c) 80 km, d) 210 km. Original images ©ESA 1994, 1996.

approximately 2 km, shortly after formation and grows to approximately 14 km as the waves approach at Palawan Island. The along crest length and number of solitons per packet also increase as the packet propagates away from its generation point. Interpacket separations, are approximately 100 km for the three packets visible in the left (April 1996) image.

The bottom right (January 1998) image shows three packets shortly after generation in the region around Pearl Bank. Current flow around Pearl Bank can reach 3.4 m/s, which generates the waves. The wave crests from these three different packets will combine to form a single packet internal wave packet that will propagate across the Sulu Sea. Wavefront variation can be seen on the left side of the middle (July 1996) image due to the effects of bathymetry.

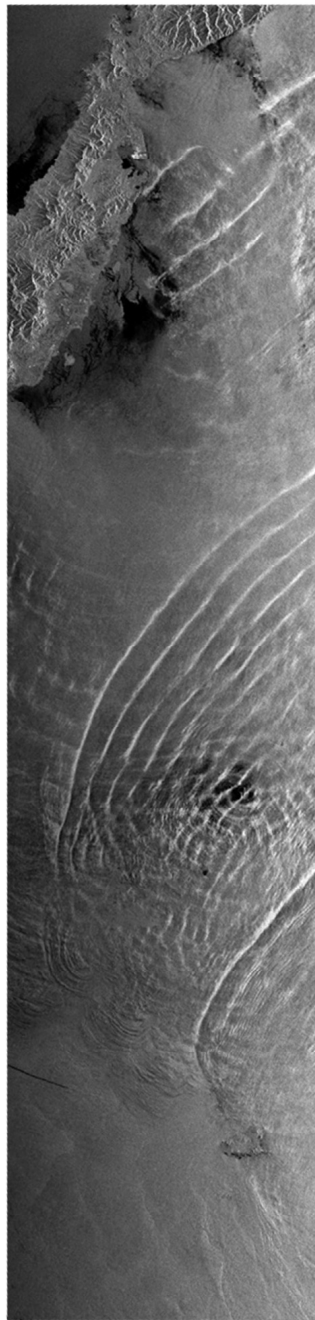


Figure 7.7. (Left/Below) Composite of ERS-1/2 (C-band, VV) imagery showing the development of internal wave packets in the Sulu Sea. The area of each frame is 100 km x 100 km. ERS images ©ESA 1996, 1998. Images courtesy of Werner Alpers: The Tropical and Subtropical Ocean Viewed by ERS SAR

Satellite	Date	Frame(s)
ERS-2	30-Jan-1998	3483
ERS-2	03-July-1996	3465 3483
ERS-1	07-Apr-1996	3411 3429 3447 3465

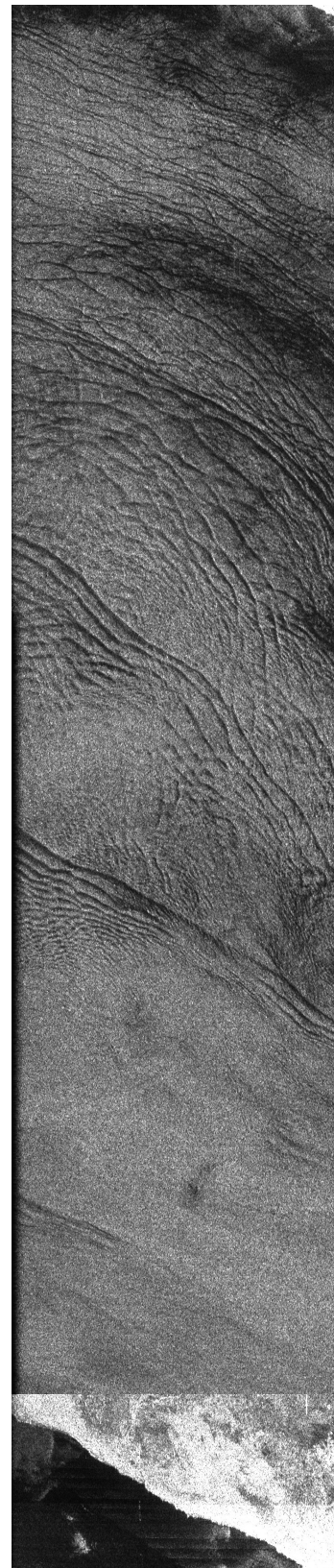
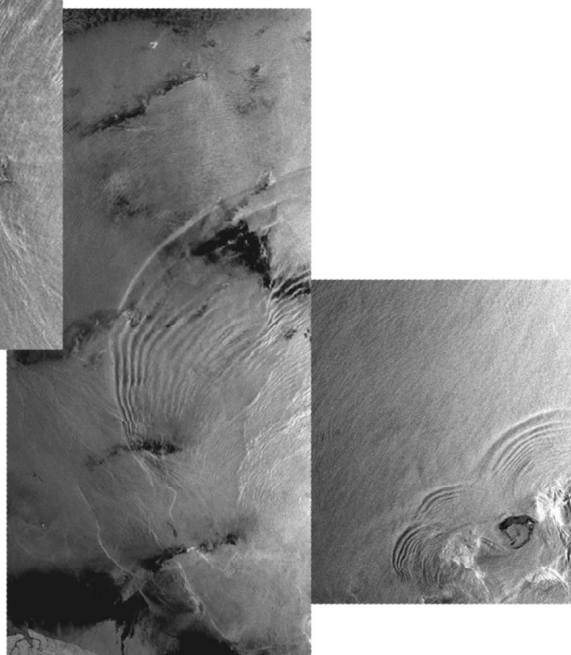


Figure 7.8. (Right) SIR-C (L-Band HH) data of internal waves off the west coast of South Africa acquired on 11 April 1994 1:22 GMT (Data Take 26.7). Imaged area is 300 km x 60 km, centered near 31°39.7'S., 16°53.1'E

Oceanic Internal Waves and Solitons

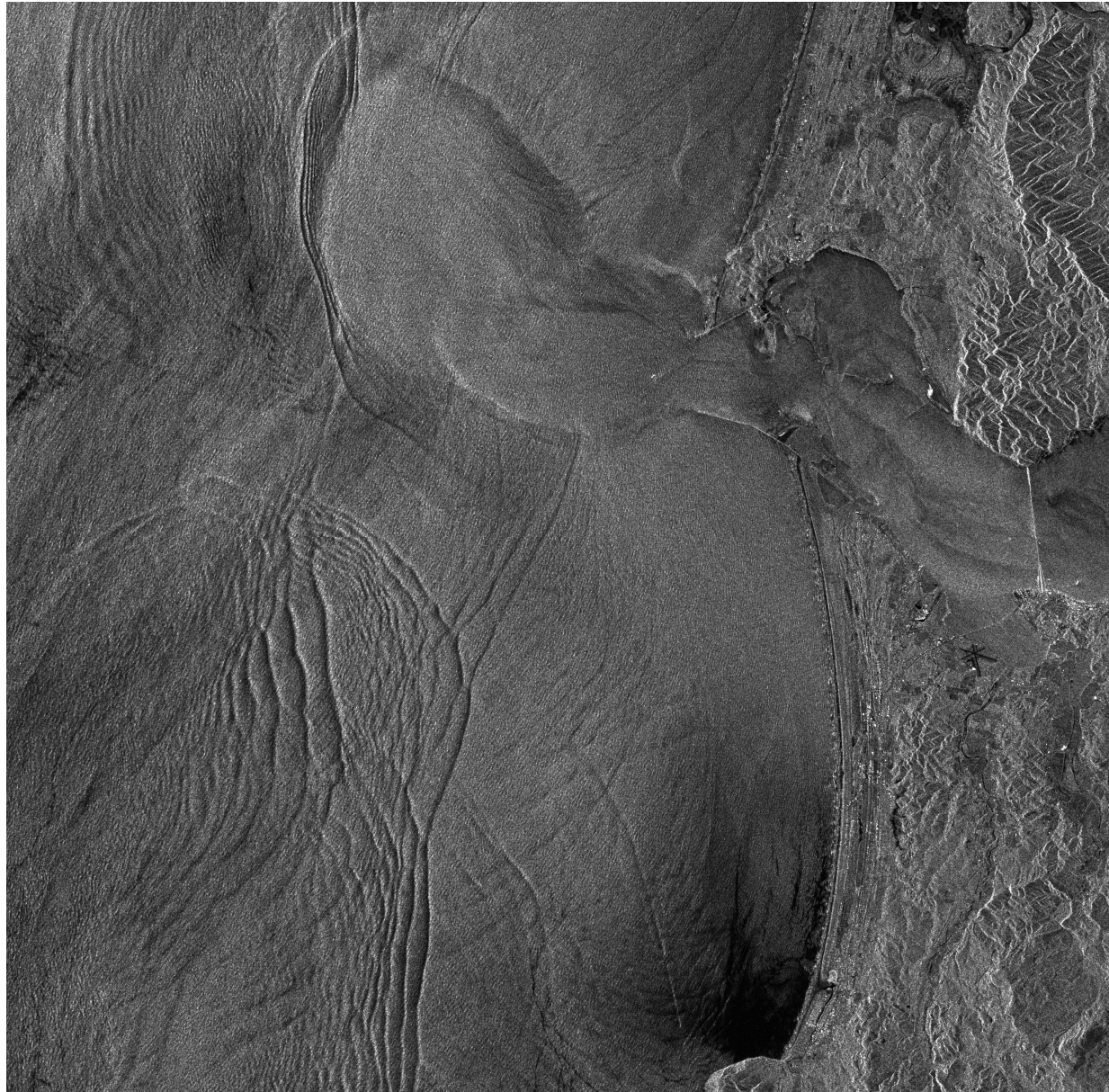


Figure 7.9. RADARSAT-1 (C-band, HH) image showing internal waves off the coast of Washington State acquired 9 August 1999 at 0155UTC. A seaward propagating wave generated by the plume of the Columbia River can be seen in addition to the usual shoreward propagating internal waves. Imaged area is 50 km x 50 km. ©CSA 1999

The left image also shows refraction effects around the San Miguel Islands where small solitons appear to be radiating away nearly orthogonal to the propagation direction of the main wave packet.

Figure 7.8 is a SIR-C (Shuttle Imaging Radar-C) C-band survey image off the west coast of South Africa taken on 11 April 1994. The internal waves along the southwest African coast have been observed between the months of November and April, which corresponds to the austral summer. The nature and character of the waves are very similar to those observed on the U.S. continental shelf in the New York Bight. Just like the New York Bight, summer heating of the upper layers in coastal waters enhances the stratification and the internal waves. The waves appear to form just inside the 200 m isobath. Interpacket separation is approximately 35 km,

which implies a propagation speed of around 0.75 m s^{-1} on the shelf. The distinction between packets disappears as they approach shore because the phase velocities of the waves are reduced by both the shoaling and (usually) by the decreasing pycnocline depth. The result is that the leading waves in one packet overtake the trailing waves in the previous packet and the interpacket boundary disappears.

While sills and continental shelves provide the most common locations for soliton generation, any disturbance penetrating the pycnocline is capable of generating internal waves. Other generation sources may include seamounts, banks, mid-ocean ridges, river and glacial outflows, and current-current interaction. Figure 7.9 presents an example of internal waves apparently generated from outflow of the Colombia River off the coast of Washington State. The image shows the usual shoreward propagating internal waves in addition to a seemingly westward propagating internal wave packet along the southwestern edge of the Colombia River plume [Clemente-Colón, 2001]. Unlike the east coast of the United States, the west coast lacks a wide continental shelf, so internal wave generation by the tides takes place closer to shore. [Fu and Holt, 1982]

7.2.3 Global Occurrences

The remotely sensed images acquired during the quarter-century since the first glimpses of oceanic solitons were obtained from the ERTS/Landsat-1 spacecraft [Apel *et al.* 1975a, 1975b; Sawyer and Apel, 1976] have allowed the construction of global maps of soliton occurrence. Figure 7.10 shows the locations of solitons observed around the world by a variety of remote and in-situ sensors. The majority of these sensors are synthetic aperture radars operated by the United States, Canada, the European Space Agency, the USSR/Russia and Japan. Indeed, SAR is the premier sensor for the detection of solitons because of its sensitivity to small surface roughness changes at ocean surface wavelengths on the order of the radar wavelength as well as its independence from cloud cover and solar illumination. In addition, SAR is a quantitative instrument because of control over factors such as frequency, phase, polarization, incidence angle, power, and swath width, all of which are important in the observation of oceanic phenomena

Figure 7.10 shows that soliton generation appears to be mostly confined to regions where relatively strong currents flow over bottom topography that protrudes up into the pycnocline. This happens mainly in coastal regions, but there are interesting and important exceptions, such as the apparent solitary waves observed near the Mid-Atlantic Ridge north of the Azores [Apel, 1987], and in packets seen with shipboard acoustic Doppler current profilers (ADCPs) northeast of the Bismarck–Solomon Islands chain in the open South Pacific [Pinkel *et al.*, 1997; Pinkel, 2000]. The Mid-Atlantic waves could be caused by the Gulf Stream extension (pycnocline depths near 600 m) flowing over the Ridge (bottom depths near 900 m), and the Pacific Island solitons were probably generated near one of the inter-island sills in the region. However, there is a dearth of open-ocean SAR imagery, so it is difficult to say how frequently deep-water solitons occur.

Nevertheless, it is clear that solitary internal waves are widespread. If the theories of internal wave generation and propagation are even approximately correct, then Internal waves should occur globally at the many locations where the combination of stratification, bathymetry, and current flow conspire to give the conditions necessary for internal wave generation. It is apparent that these conditions are common especially during the summer months in water of less than a few hundred meters depth. Internal solitons, then, are likely to be ubiquitous.

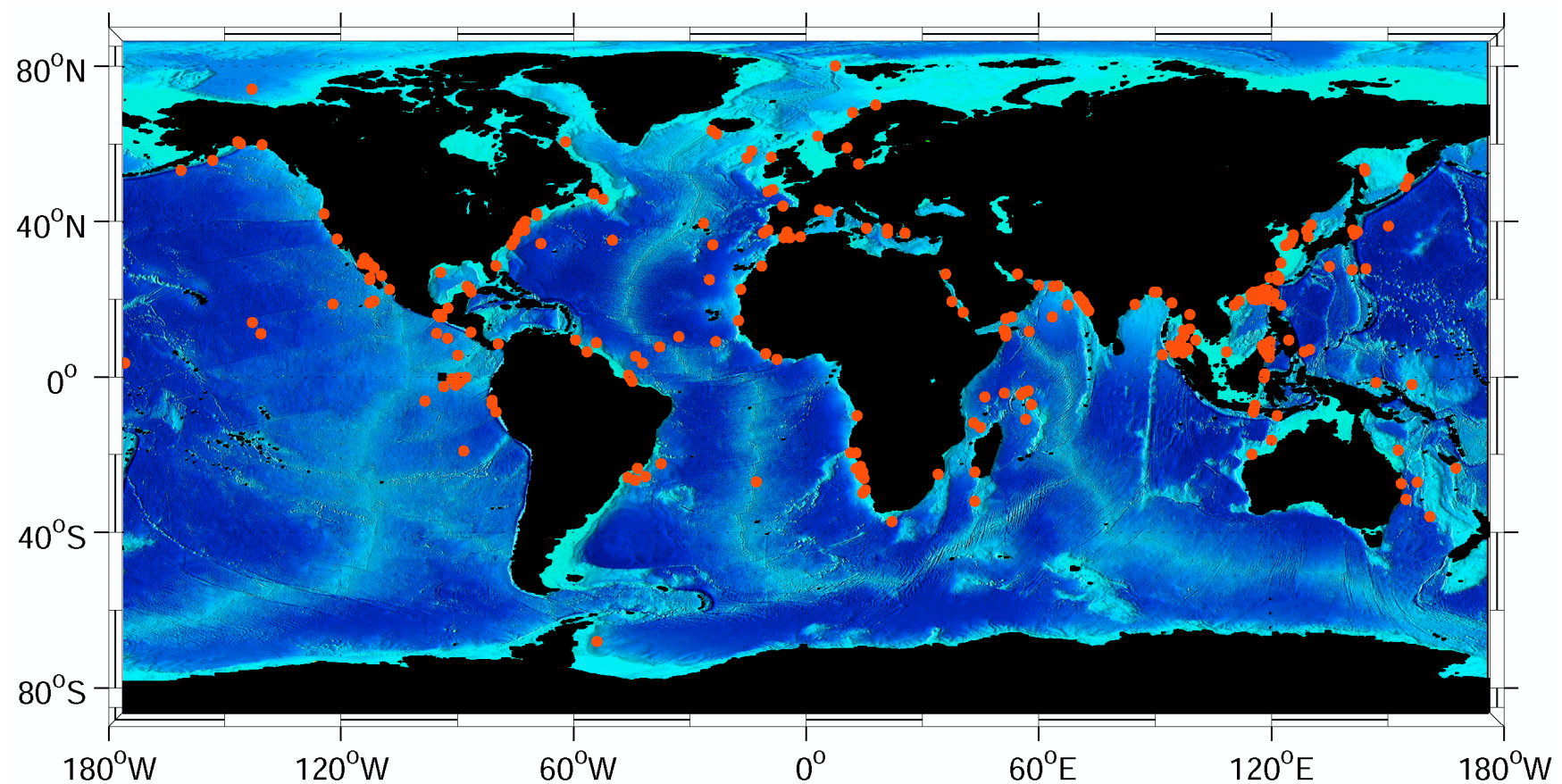


Figure 7.10. Locations of observed soliton occurrences around the world. Most locations were detected in satellite imagery. As additional data and imagery are collected, the number of noted occurrence locations will certainly increase.

7.3 Summary

Internal waves are among the most easily recognized of the oceanographic phenomena observed in remote sensing imagery. The characteristic signature of alternating bands of light and dark quasilinear strips have been noted in photographs of the sea surface, in multispectral radiometer images, and in real and synthetic aperture radar images.

It has been nearly four decades since the first in-situ observations were made of nonsinusoidal waveshapes for internal waves on the continental shelf [LaFond, 1962]. However, it has only been since satellite images have been acquired in sufficient quantity that the global extent and the recurrence of the waves have been appreciated. In this regard, the accumulation of some ten years of SAR data from ERS-1, ERS-2, and Radarsat-1 has added greatly to the limited but tantalizing pictures from LANDSAT [Sawyer and Apel, 1976] and SEASAT [Fu and Holt, 1982].

Internal solitons are among the most coherent and reproducible phenomena in the sea, barotropic astronomical tides perhaps excepted. Since tidal currents are one ingredient in the recipe for producing most observed solitons (others being stratification and variable bathymetry that perturbs the density structure), it is not surprising that solitons follow the tides and the seasons.

The characterization of soliton packets as oscillations on the leading edge of the nonlinear internal tide is more recent [Gerkema, 1994, 1996; Apel, 1998]. Viewed from this perspective, the solitons can be regarded as part of the response of a fluid to an imposed internal shock, that is, they are a “ringing” of the leading edge of a super-Froude shock front moving across the ocean and repeating every 12½ hours. This front transports mass and momentum in both its mean and its fluctuations. The other part of the response lies in the recovery from the initial downward displacement of the density field during the remainder of the tidal cycle. The inclusion of Coriolis effects, which has not been mentioned here in detail, has an inhibiting influence on the onset of oscillations [Gerkema, 1994].

Differences and similarities between solitons generated at shelf breaks and sills are pointed out, with the water depth in the far field being important to the lifetime of the waves. Packets generated at sills appear on the average to be more energetic than those generated at shelf breaks, and to take on more of the characteristics of solibores [Henyey and Hoering, 1997]; this is probably related to the intensity of tidal flows near sills. The exact mechanisms for generation are not yet established, but the two main hypotheses, lee-wave formation and barotropic–baroclinic scattering, seem to happen at various locales. This is a first-order problem for future research. The relative magnitude of the various dissipation mechanisms are also unknown. This difficult problem is also a first-order research issue that is important to resolve because of its impact on oceanic optical opacity, nutrification, and bio-stimulation.

7.4 References

- Alpers, W., 1985: Theory of radar imaging of internal waves. *Nature*, **314**, 245–247.
- , W. C. Heng, and H. Lim, 1997: Observation of internal waves in the Andaman Sea by ERS SAR. *Third ERS Symp. on Space at the Service of Our Environment*, Florence, Italy, ESA, 1287–1291.
- Apel, J. R., 1979: Observations of internal wave surface signatures in ASTP photographs. *Apollo-Soyuz Test Project Summary Science Report*, F. El-Baz and D. M. Warner, Eds., NASA Publication SP-412, 505–509.

- , 1987: *Principles of Ocean Physics*. Academic Press, 634 pp.
- , 1998: Comparisons between the dnoidal soliton model and observations. *Proceedings of the Fourth Pacific Ocean Remote Sensing Conference (PORSEC)*, M.-X. He and G. Chen, Eds., Vol. 1, PORSEC'98 Secretariat, 444–447.
- , 2000: *Solitons near Gibraltar: Views from the European Remote Sensing Satellites*. Global Ocean Associates, 23 pp.
- , and J. R. Holbrook, 1983: Internal solitary waves in the Sulu Sea. *Johns Hopkins APL Tech. Dig.*, 4, 267–275.
- , and P. F. Worcester, 2000: Internal solitons near Gibraltar: A longitudinal study using ERS-1 and 2 SAR imagery. *Proc. ERS-Envisat Symp.: Looking Down to Earth in the New Millennium*, Gothenburg, Sweden, European Space Agency.
- , J. R. Proni, H. M. Byrne, and R. L. Sellers, 1975a: Near-simultaneous observations of intermittent internal waves on the continental shelf from ship and aircraft. *Geophys. Res. Lett.*, 2, 128–131.
- , H. M. Byrne, J. R. Proni, and R. L. Charnell, 1975b: Observations of oceanic internal and surface waves from the Earth Resources Technology Satellite. *J. Geophys. Res.*, 80, 865–881.
- , J. R. Holbrook, J. Tsai, and A. K. Liu, 1985: The Sulu Sea internal soliton experiment. *J. Phys. Oceanogr.*, 15, 1625–1651.
- , and Coauthors, 1997: An overview of the 1995 SWARM Shallow-Water Internal Wave Acoustic Scattering Experiment. *IEEE J. Oceanic Eng.*, 22, 465–500.
- Armi, L., and D. M. Farmer, 1988: The flow of Mediterranean water through the Strait of Gibraltar. *Progress in Oceanography*, Vol. 21, Pergamon, 1–105.
- Brandt, P., W. Alpers, and J. O. Backhaus, 1996: Study of the generation and propagation of internal waves in the Strait of Gibraltar using a numerical model and synthetic aperture radar images of the European ERS 1 satellite. *J. Geophys. Res.*, 101, 14 237–14 252.
- Clemente-Colón, P., 2001: Coastal oceanography applications of spaceborne Synthetic Aperture Radar (SAR) in the Middle Atlantic Bight (MAB). Ph.D. dissertation, College of Marine Studies, University of Delaware, 233 pp.
- Elachi, C. and J.R. Apel, 1976: Internal Wave Observations Made with an Airborne Synthetic Aperture Radar. *Geophys. Res. Lett.*, 3, 647–650.
- Ekman, V. W., 1904: On dead water. *Sci. Results Norw. North Polar Exped. 1893–96*, 5, 1–152.
- Farmer, D. M., and L. Armi, 1988: The flow of Atlantic water through the Strait of Gibraltar. *Progress in Oceanography*, Vol. 21, Pergamon, 1–105.
- Fu, L. L., and B. Holt, 1982: Seasat views oceans and sea ice with synthetic aperture radar. JPL Publication 81-120, Pasadena CA, 200 pp.
- Gasparovic, R.F. and V. S. Etkin, 1994: An overview of the Joint US/Russian internal wave remote sensing experiment. *Proc. 1994 Int. Geoscience and Remote Sensing Symp. (IGARSS94)*, Pasadena, California, IEEE, 741–743.
- , J. R. Apel, and E. S. Kasischke, 1988: An overview of the SAR internal wave signature experiment. *J. Geophys. Res.*, 93C, 12 304–12 316.
- Gerkema, T., 1994: Nonlinear dispersive tides: Generation models for a rotating ocean. Ph.D. dissertation, Netherlands Institute for Sea Research, 149 pp.
- , 1996: A unified model for the generation and fission of internal tides in a rotating ocean. *J. Mar. Res.*, 54, 421–450.

- Henyey, F. S., and A. Hoering, 1997: Energetics of borelike internal waves. *J. Geophys. Res.*, **102**, 3323–3330.
- Hsu, M.-K., A. K. Liu, and C. Liu, 2000a: A study of internal waves in the China Seas and Yellow Sea using SAR. *Contin. Shelf Res.*, **20**, 389–410.
- Hsu, M.-K., and A. K. Liu, 2000b: Nonlinear internal waves in the South China Sea. *Can. J. Remote Sens.*, **26**, 72–81.
- IOC, IHO, and BODC, 1997: GEBCO-97: The 1997 edition of the GEBCO digital atlas. British Oceanographic Data Centre, National Environmental Research Council.
- Korteweg, D. J., and G. de Vries, 1895, “On the change of form of long waves advancing in a rectangular canal, and on a new type of long stationary wave,” *Phil. Mag.*, **39**, Ser. 5, 422–443.
- Lafond, E. C., 1962: Internal waves. *The Sea*, M.N. Hill, Ed., Physical Oceanography, Vol. 1, Wiley and Sons, 731–751.
- Liu, A. K., J. R. Holbrook, and J. R. Apel, 1985: Nonlinear internal wave evolution in the Sulu Sea. *J. Phys. Oceanogr.*, **15**, 1613–1624.
- , Y. S. Chang, M.-K. Hsu, and N. K. Liang, 1998: Evolution of nonlinear internal waves in the East and South China Seas. *J. Geophys. Res.*, **103**, 7995–8008.
- Osborne, A. R., and T. L. Burch, 1980: Internal solitons in the Andaman Sea. *Science*, **208**, 451–460.
- Pinkel, R., 2000: Internal solitary waves in the warm pool of the western equatorial Pacific Ocean. *J. Phys. Oceanogr.*, **30**, 2906–2926.
- , M. Merrifield, M. McPhaden, J. Picaut, S. Rutledge, D. Siegel, and L. Washburn, 1997: Solitary waves in the western Equatorial Pacific Ocean. *Geophys. Res. Lett.*, **24**, 1603–1606.
- Russell, J. S., 1838: Report to committee on waves. *Report of the 7th Meeting of the British Association for the Advancement of Science*, Liverpool, United Kingdom, British Association for the Advancement of Science, 417–496.
- , 1844: Report on waves. *Report of the 14th Meeting of the British Association for the Advancement of Science*, York, United Kingdom, British Association for the Advancement of Science, 311–390.
- Sawyer, C., and J. R. Apel, 1976: Satellite images of oceanic internal wave signatures. National Oceanic and Atmospheric Administration, Environmental Research Laboratories, NOAA S/T-2401.
- Smith, W. H. F., and D. T. Sandwell, 1997: Global seafloor topography from satellite altimetry and ship depth soundings, *Science*, **277**, 1957–1962.
http://topex.ucsd.edu/marine_topo/mar_topo.html
- Wallace, A. R., 1869: *The Malay Archipelago*. Dover Publications, 370–374.
- , 1922: *The Malay Archipelago*. Dover Publications, 410–413